Thin Solid Films 519 (2011) 6026–6032

Contents lists available at ScienceDirect

Thin Solid Films

journal homepage: www.elsevier.com/locate/tsf

Vibrational characteristics of bilayer graphene sheets

Y. Chandra [a], R. Chowdhury [a], F. Scarpa [b], S. Adhikaricor [a,*]

[a] Multidisciplinary Nanotechnology Centre, Swansea University, Swansea SA2 8PP, United Kingdom
[b] Advanced Composites Centre for Innovation and Science, University of Bristol, Bristol BS8 1TR, United Kingdom

ARTICLE INFO

Article history:
Received 21 September 2010
Received in revised form 1 April 2011
Accepted 5 April 2011
Available online 13 April 2011

Keywords:
Bilayer graphene sheets
Nanodynamics
Atomistic model
Natural frequencies

ABSTRACT

Bilayer graphene sheets (BLGSs) are currently receiving increasing attention. In this paper, the vibration characteristics of BLGSs are investigated using analytical and atomistic finite element approaches. Various possible scenarios, namely different geometrical configuration (armchair and zigzag), boundary conditions, and aspect ratio are considered in the present study. The dynamic characteristics of BLGS studied have shown dependence on aspect ratio and the boundary conditions. The unique vibrational properties and large stiffness of BLGS identified in the present work make them suitable candidates for manufacturing nanosensors; electromechanical resonators also will aid the nanomaterials research community to design nanodevices.

1. Introduction

Growing research interest in the application of carbon nanostructures has emerged since the discovery of superlattice monolayers and thin films in graphite [1,2], also denominated as graphene [3–6]. Graphene has attracted tremendous attention in both its 2D and 1D forms, the latter being obtained by patterning the layer into strips or ribbons [7]. In an experimental work in 2004, Meyer et al. [8] reported the possibility of suspending single-layer graphene sheets (SLGSs) in vacuum, e.g., the possibility of bilayer graphene sheets (BLGSs). BLGSs are two atom thick array of carbon sp^2 bonds forming a double layer SLGS, with an inter layer width of 0.34 nm [9–11]. Bilayer graphene has been proposed as the only semiconductor to produce insulating state and switch-off electrical conduction [12,13]. Another unusual property associated to this nanostructure is the presence of two structural domains at 180° when grown on SiC substrate, showing a "shifted stacking" of the layers due to lattice mismatch induced by the roughness of the silicon carbide [14]. Pal and Gosh [15,16] have investigated the low-frequency electrical resistance fluctuations in bilayer and multilayer graphenes. Although the mechanical properties of SLGSs (stiffness and natural frequencies) have been studied by many authors [9–11,17–22], limited literature exists for the case of double and multi-layered graphene structures [21,23–28]; experimental data on the out-of-plane properties of multilayer graphene have been obtained by Frank et al. [29]. Behfar and Naghdabadi [28] investigated the nanoscale vibration of a multi-layered graphene sheet embedded in an elastic medium, in which the natural frequencies as well as the associated modes were determined using a continuum-based model. In line with this study, Liew et al. [27] derived a set of explicit formulas for the natural frequencies and the associated modes for double- and triple-layered graphene sheets embedded in an elastic matrix.

The authors have recently formulated a modeling approach, where the equivalent homogenized properties of a graphene sheet are expressed in terms of the thickness, equilibrium lengths, and force-field models used to represent the C—C bonds of the graphene lattice [17]. The covalent bonds are represented as structural beams with stretching, bending, torsional and deep shear deformations, based on the equivalence between the harmonic potential expressed in terms of Morse and Amber models [30], and the strain energies associated to affine deformation mechanisms. The overall mechanical properties and geometric configurations of the nanostructures represented as truss assemblies (finite elements) are then calculated minimizing the total potential energy associated to the loading, thickness, and average equilibrium lengths of the bonds. In the present work, we have focused on the nanoscale dynamics of BLGS. A typical example of a BLGS is shown in Fig. 1. Various possible scenarios, namely different geometrical configurations (armchair and zigzag), boundary conditions, and aspect ratio are considered in the present study. We propose also an analytical plate model to simulate in a compact form the mechanical vibrational behavior of BLGS, providing a further benchmark to the atomistic finite element (FE) model of the bilayer graphene.

The paper is organized in the following way. The continuum mechanics approach for the frequency analysis of graphene sheets is presented in Section 2. Section 3 will be centered on the modeling, analysis, and calculation of the frequencies using atomistic FE

* Corresponding author. Tel.: +44 1792 602088; fax: +44 1792 295676.
E-mail address: S.Adhikari@swansea.ac.uk (S. Adhikaricor).

0040-6090/$ – see front matter © 2011 Elsevier B.V. All rights reserved.
doi:10.1016/j.tsf.2011.04.012

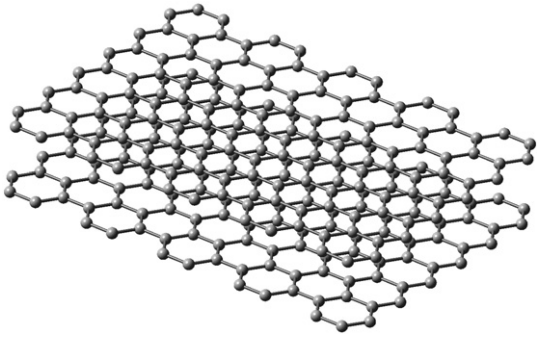

Fig. 1. Bilayer graphene sheet: atomic configuration of width = 19.074 Å and length = 19.538 Å.

approach. The numerical results and discussion will be presented in Section 4. Finally, the major conclusions of this paper will be drawn in Section 5 based on the results and analyses in Section 4.

2. Vibration of bilayer graphene

For the monolayer graphene sheets, linear as well as nonlinear [31] elasticity models have been proposed. At its simplest approximation, a bilayer graphene sheet may be represented by an elastic plate with an equivalent thickness. The governing equation of motion of an elastic plate undergoing flexural vibration can be given as [32–35]:

$$D\left(\frac{\partial^4 w}{\partial x^4} + 2\frac{\partial^2 w}{\partial x^2}\frac{\partial^2 w}{\partial y^2} + \frac{\partial^4 w}{\partial y^4}\right) + \rho\frac{\partial^2 w}{\partial t^2} = 0 \tag{1}$$

where $w \equiv w(x, y, t)$ is the deflection distributed over the x, y coordinates of the plate, t is the time, ρ is the mass density. The bending rigidity (D) is given by

$$D = \frac{E(h + 2d)^3}{12(1-\nu^2)} \tag{2}$$

The bending rigidity is governed by the Young's modulus E, the interlayer distance h, the thickness d of each SLGS, and the Poisson's ratio ν of the equivalent graphene material. The natural frequency for an elastic plate of dimensions $a \times b$ is given by [36]:

$$\omega_{ij} = \left\{\frac{\pi^4 D}{a^4\rho}\right\}^{1/2}\left\{G_x^4 + G_y^4\left(\frac{a}{b}\right)^4 + 2\left(\frac{a}{b}\right)^2\left[\nu H_x H_y + (1-\nu)J_x J_y\right]\right\}^{1/2} \tag{3}$$

where i, $j = 1, 2, 3, \ldots$ are mode indices. The values of the coefficients G_x, H_x, J_x and G_y, H_y, J_y for three different boundary conditions are given in Table 1.

From a structural mechanics point of view, the BLGS forms a composite structure involving Lennard–Jones (L–J) potential sandwiched (the "core") between two graphene sheets [23]. One can estimate the equivalent Young's modulus E_{eq} of the bilayer using the standard rule of mixture for unidirectional composites [37] and neglecting the stiffness contribution of the L–J potential:

$$E_{eq} = E_{Graphene}\left[\frac{1}{1 + \left(\frac{h}{2d}\right)}\right]. \tag{4}$$

The equivalent Young's modulus has been considered for the calculation of elastic plate natural frequencies using Eq. (3).

Table 1
Coefficients for the various boundary conditions.

BC	i	j	G_x	H_x	J_x	G_y	H_y	J_y
Cantilever (CFFF)	1	0	0.597	−0.087	0.471	0.0	0.0	0.0
Bridged (CCFF)	1	0	1.506	1.248	1.248	0.0	0.0	0.0
Simply supported (SSSS)	1	0	1	1	1	1	1	1

3. Atomistic finite element approach

3.1. Modeling of carbon—carbon covalent bonds

The carbon—carbon sp^2 bonds can be considered as equivalent beams having axial, out-of-plane, and in-plane rotational deformation mechanisms. The harmonic potential associated to the C—C bond can be expressed as [11]:

$$U_r = \frac{1}{2}k_r(\delta r)^2 \quad U_\theta = \frac{1}{2}k_\theta(\delta\theta)^2 \quad U_\tau = \frac{1}{2}k_\tau(\delta\varphi)^2. \tag{5}$$

The equivalent mechanical properties of the C—C bond can be calculated using a beam mapping technique, imposing the equivalence between the harmonic potential and the mechanical strain energies of a hypothetical structural beam of length L [17]:

$$\frac{k_r}{2}(\delta r)^2 = \frac{EA}{2L}(\delta r)^2 \tag{6}$$

$$\frac{k_\tau}{2}(\delta\varphi)^2 = \frac{GJ}{2L}(\delta\varphi)^2 \tag{7}$$

$$\frac{k_\theta}{2}(\delta\theta)^2 = \frac{EI}{2L}\frac{4 + \Phi}{1 + \Phi}(\delta\theta)^2 \tag{8}$$

Eq. (6) corresponds to the equivalence between stretching and axial deformation mechanism (with E being the equivalent Young's modulus), while Eq. (7) equates the torsional deformation of the C—C bond with the pure shear deflection of the structural beam associated to an equivalent shear modulus G. Contrary with similar approaches previously used [11,22], the term equating the in-plane rotation of the C—C bond (Eq. (8)) is equated to a bending strain energy related to a deep shear beam model, to take into account the shear deformation of the cross section. The shear correction term becomes necessary when considering beams with aspect ratio lower than 10 [32]. For circular cross sections, the shear deformation constant can be expressed as [17]:

$$\Phi = \frac{12EI}{GA_s L^2}. \tag{9}$$

In Eq. (9), $A_s = A/F_s$is the reduced cross section of the beam by the shear correction term F_s [38]:

$$F_s = \frac{6 + 12\nu + 6\nu^2}{7 + 12\nu + 4\nu^2} \tag{10}$$

The insertion of Eqs. (9) and (10) in (2) leads to a nonlinear relation between the thickness d and the Poisson's ratio ν of the equivalent beam [17]:

$$k_\theta = \frac{k_r d^2}{16}\frac{4A + B}{A + B} \tag{11}$$

where

$$A = 112L^2k_\tau + 192L^2k_\tau\nu + 64L^2k_\tau\nu^2 \tag{12}$$

$$B = 9k_r d^2 + 18k_r d^4\nu + 9k_r d^4\nu^2. \tag{13}$$

For the values for the force constants for the Morse model, we adopt $k_r = 8.74\times10^{-7}\,\mathrm{Nmm^{-1}}$, $k_\theta = 9.00\times10^{-10}\,\mathrm{Nnmrad^{-2}}$, and $k_\tau = 2.78\times10^{-10}\,\mathrm{Nnm^{-1}rad^{-2}}$. The equivalent mechanical properties of the C—C bond can be determined performing a nonlinear optimization of Eqs. (6)–(8) using a Marquardt algorithm [39]. The C—C bond can then be discretized as a single two-node, three-dimensional FE model beam with a stiffness matrix described in reference 40, where the nodes represent the atoms. The atomistic and lattice models of the square graphene sheets are assembled using the FE discretization as presented in Fig. 1. In the lattice model, at each substep of the Newton–Raphson solver technique [41], the total potential energy is minimized to identify the thickness of the C—C bonds and the average equilibrium length of the covalent bonds. The nonlinear minimization technique is performed in two steps, with a zero order method to identify first the minimal clusters and a subsequent first order derivative-based method to identify the absolute minimum of the potential energy. For a comprehensive understanding of the above procedure, readers are referred to references 17,20,23.

In the atomistic FE approach, BLGSs are modeled as space-frame structures (Fig. 1). Overall mass and stiffness matrices of the atomistic FE models are generated from the equivalent matrices of the beams representing C—C bonds and concentrated masses at each node. The lumped mass matrix for a single beam element can be represented as:

$$[\mathbf{M}]_\mathbf{e} = \mathrm{diag}\left[\frac{m_c}{3}\quad\frac{m_c}{3}\quad\frac{m_c}{3}\quad 0\quad 0\quad 0\right], \tag{14}$$

where $m_c = 1.9943\times10^{-26}\,\mathrm{kg}$ is the mass of a carbon atom [9]. The general equation of motion of the undamped system ($[\mathbf{K}]\mathbf{x} + [\mathbf{M}]\ddot{\mathbf{x}} = 0$) leads to a standard undamped eigenvalue problem ($([\mathbf{K}]-\omega^2[\mathbf{M}])\{\mathbf{x}\} = \{0\}$), which has been solved using a block Lanczos algorithm.

3.2. Modeling the interlayer potential

The equivalent axial force related to the L–J potential between pair of atoms (i, j) belonging to different graphite layers can be expressed as [23]:

$$F_{ij} = \frac{\partial V_{ij}}{\partial r} \tag{15}$$

where r is the atomic displacement along **ij** (layer–layer length). According to Girifalco et al. [42], the force between the atoms (ij) can also be represented by:

$$F_{ij} = -12\epsilon\left[\left(\frac{r_{\min}}{y}\right)^{13} - \left(\frac{r_{\min}}{y}\right)^{7}\right] \tag{16}$$

where $y = r_{\min} + \delta r$, δr is the atomic displacement along the length **ij**. The $r_{\min}$ (in Å) is given by $2^{\frac{1}{6}}\sigma$, where $\sigma = (A/B)^{1/6}$. The B and A are attractive and repulsive constants, and for our cases of boundary conditions, they are given by $24.3\times10^3 eV\times Å^{12}$ and $15.4\,eV\times Å^6$, respectively, and ϵ is $B^2/(4A)$. In the atomistic models, we have used spring elements to form a nonlinear connection between two layers of the bilayer structure representing L–J potentials. The force deflection curve for L–J springs has been calculated by using the relation in Eq. (16).

3.3. Boundary conditions

Since the atomic configurations can have a significant impact on the mechanical properties of graphene sheets, zigzag and armchair models [9,18] are adopted in this study. The zigzag and armchair models of the graphene sheets under consideration are as follows:

- BLGS1: armchair model clamped at one edge (cantilevered condition)
- BLGS2: armchair model clamped at two opposite edges (bridged condition)
- BLGS3: zigzag model clamped at one edge (cantilevered condition)
- BLGS4: zigzag model clamped at two opposite edges (bridged condition)

Schematic diagrams of the four BLGS models are shown in Fig. 2.

4. Results and discussions

The resonant frequencies of SLGS and BLGS based resonators depend on the geometric configurations. The atomic structures of SLGS and BLGS could also exert significant influence on their vibration behaviors. Thus, in this work, we analyze two groups of resonators, i.e., zigzag and armchair with varying length and width. An initial free–free modal simulation has been carried out to verify the dynamic behavior of the bilayer structure without the influence of external clamps and/or supports. The four mode shapes of cantilever and bridged SLGS are given in Figs. 3 and 4, respectively. The first four mode shapes for the cases BLGS1 and BLGS2 are presented in Figs. 5 and 6, respectively. We have chosen a model with aspect ratio of 4 and width of 1.49 nm, for the purpose of demonstrating vibration modes. In both cases (BLGS1 and BLGS2), the first two modes are flexural while the third is constituted by an out-of-plane torsional. It was observed that the first four mode shapes related to BLGS1 and BLGS2 are identical with those associated to BLGS3 and BLGS4 nanostructures. Also, the corresponding mode shapes of SLGS are found to be similar to those of BLGS, for both the boundary conditions.

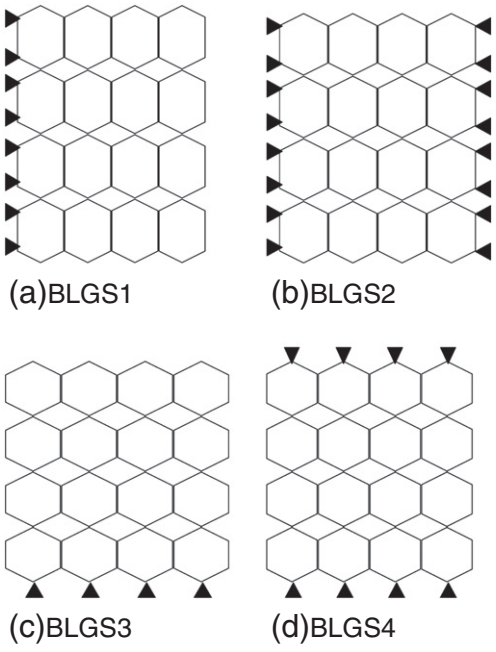

Fig. 2. Four BLGS models: BLGS1 = armchair cantilevered, BLGS2 = armchair bridged, BLGS3 = zigzag cantilevered, BLGS4 = zigzag bridged. The triangular gaps will not occur in an actual sheet.

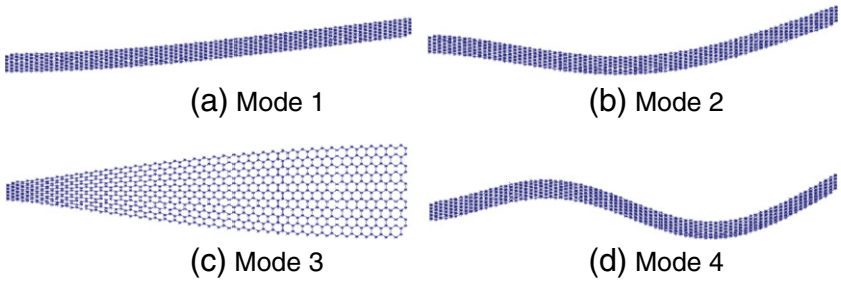

Fig. 3. The first four mode shapes of cantilever SLGS with aspect ratio of 4 and width of 1.49 nm: (a) mode 1, bending; (b) mode 2, bending; (c) mode 3, out-of-plane twisting; (d) mode 4, bending.

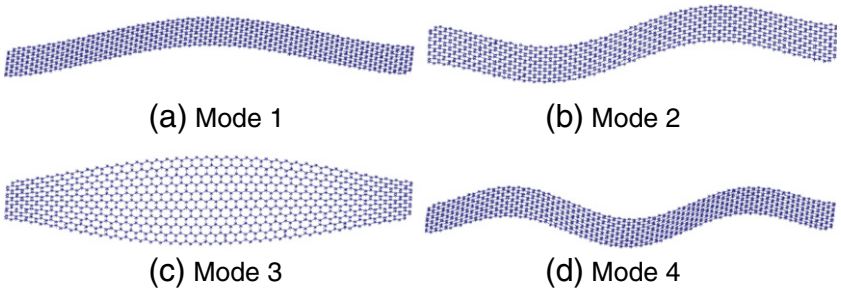

Fig. 4. The first four mode shapes of bridged SLGS with aspect ratio of 4 and width of 1.49 nm: (a) mode 1, bending; (b) mode 2, bending; (c) mode 3, out-of-plane twisting; (d) mode 4, bending.

4.1. Dependence on the length and aspect ratio

The results related to the fundamental frequencies of armchair and zigzag BLGS are presented in Fig. 7, for bridged and cantilevered boundary condition. One can observe that armchair BLGS (width = 4.33 nm) with the increasing length from ~15 Å to ~140 Å have fundamental frequencies in the range between 25 and 470 GHz and 80 and 1110 GHz. Zigzag BLGS (width = 4.06 nm) have instead their natural frequencies distributed between 23 and 300 GHz and 75 and 770 GHz for cantilevered and bridged boundary conditions, respectively, this time with increasing lengths between 20 Å and 120 Å. The trend observed (Fig. 7) is similar to the one identified for SLGS [9]. However, BLGS does show an increase of the fundamental frequency by a factor around 4 for a given aspect ratio. In our atomistic-FE model, the BLGS nanostructure behaves at first approximation as a sandwich beam, a mechanical behavior consistent with the one observed under static loading, and benchmarked against experimental results [23]. From these results, we can assume that the percentage decreases of the natural frequency follows a series of increasing powers (a, ar^2, ar^3, ar^4.....), where the scale factor a is the natural frequency associated to the lowest considered length. The common ratio r is found to be approximately between 0.6 and 0.5.

In Fig. 8, the variations of natural frequencies with respect to length at a given aspect ratio are shown. The plots in Fig. 8 are similar to the ones obtained by Sakhaee-Pour et al. [9] for SLGS, suggesting that the pattern related to the variation of the natural frequencies versus the nanostructure length is identical for SLGS and BLGS structures. In Fig. 8, the first value of the frequency associated to an aspect ratio (AR) of 1.15 coincides with the second natural frequency for AR = 0.57, i.e., at width reduction of about 50%.

4.2. Dependence on the boundary condition

The bridged structure generally offers higher natural frequency [35] as compared to the cantilever one. Referring to Fig. 7, the change of the boundary condition from one-edge-fixed to both-edge-fixed

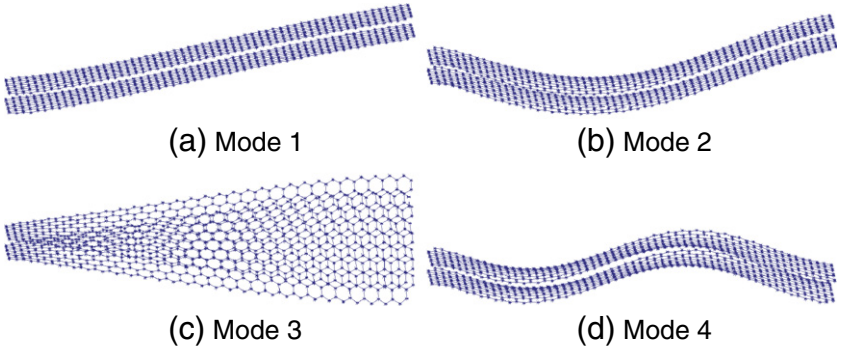

Fig. 5. The first four mode shapes of BLGS1 with aspect ratio of 4 and width of 1.49 nm: (a) mode 1, bending; (b) mode 2, bending; (c) mode 3, out-of-plane twisting; (d) mode 4, bending.

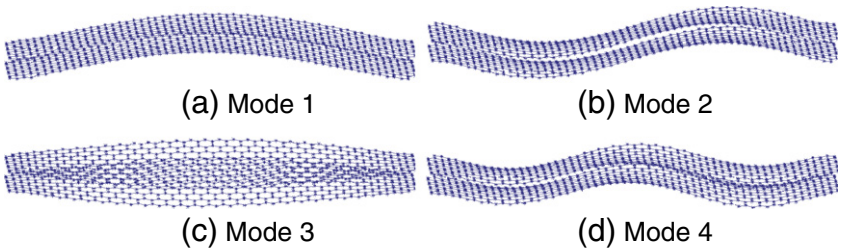

Fig. 6. The first four mode shapes of BLGS2 with aspect ratio of 4 and width of 1.49 nm: (a) mode 1, bending; (b) mode 2, bending; (c) mode 3, out-of-plane twisting; (d) mode 4, bending.

increases the fundamental frequency to about three times. We have observed a similar trend for the second natural frequency also. Clamping the BLGS at all edges will further enhance the stiffness and consequently increase the natural frequency. These results suggest that, with the increasing of the aspect ratio, the natural frequency of a cantilever model will be lowered at higher rate compared to a bridged BLGS. From these observations, we can also conclude that the models associated to BLGS2 and BLGS4 topologies are suitable for nano-electro-mechanical-system applications, where resonant frequencies are required to be very high [43–45], whereas the models BLGS1 and BLGS3 are suitable for low resonant frequency applications.

4.3. The effect of chirality

Chirality and aspect ratio have a significant influence on the natural frequencies of vibration (Fig. 7). For almost identical widths and lengths, the fundamental frequencies of armchair BLGS are higher than the

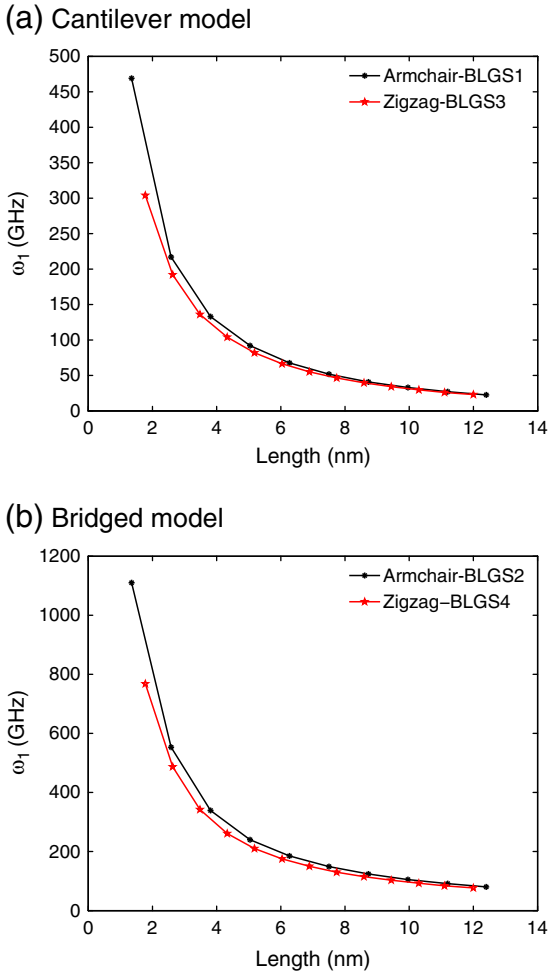

Fig. 7. The dependence of the natural frequency with length: (a) cantilevered boundary condition, fundamental frequencies of armchair and zigzag BLGS as a function of the length of BLGS. The widths are as follows: BSLGS1, 4.33 nm; BLGS3, 4.06 nm; (b) bridged boundary condition, fundamental frequencies of armchair and zigzag BLGS as a function of the length of BLGS. The widths are as follows: BLGS2: 4.33 nm; BLGS4, 4.06 nm.

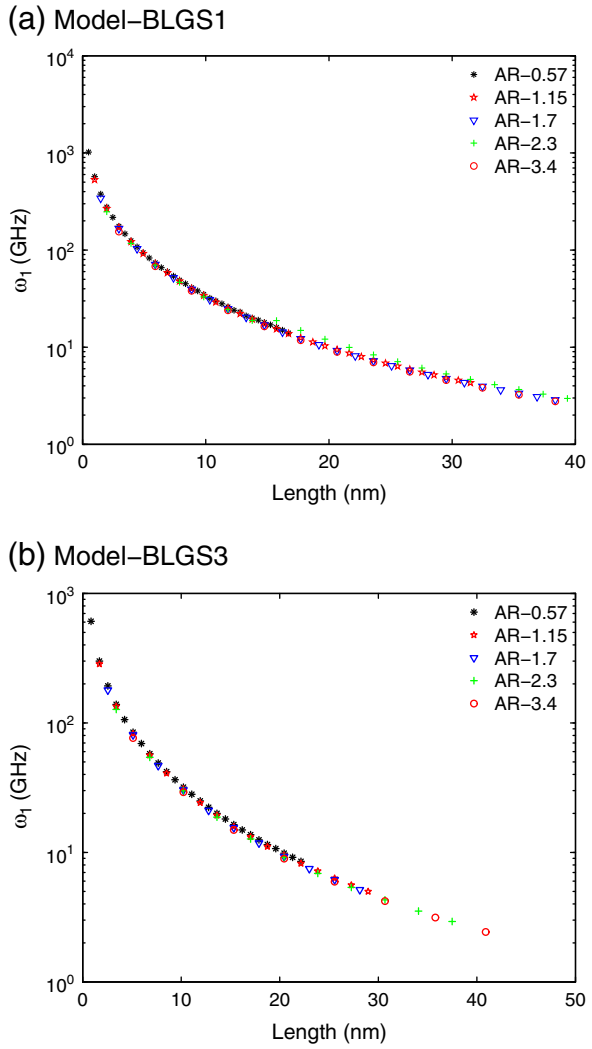

Fig. 8. The variation of natural frequencies with length at a given aspect ratio.

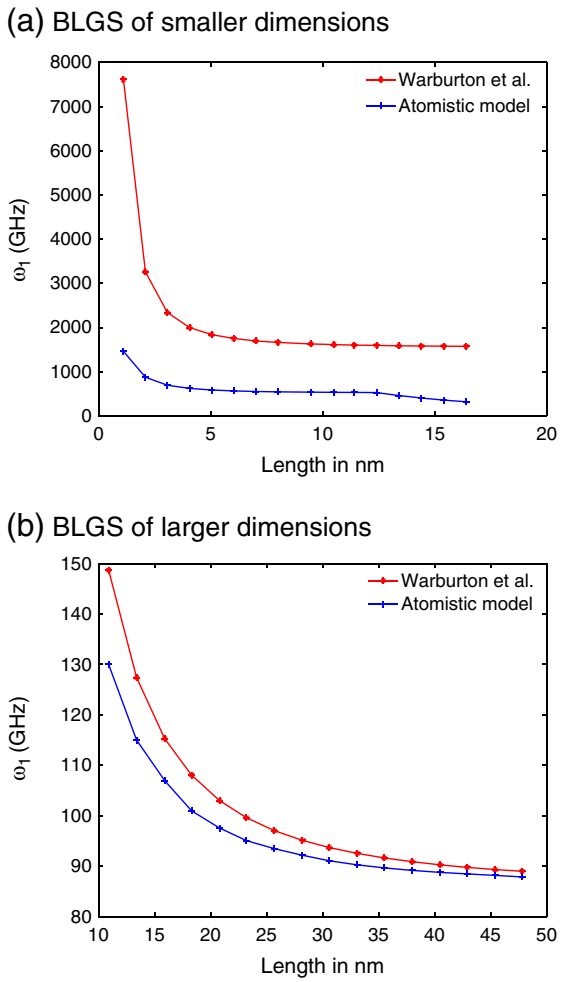

Fig. 9. Simply supported boundary condition—fundamental vibrational frequencies of the BLGS. Atomistic FE results and continuum mechanics results are compared for different values of the length. Considerable error (~18%) occurred for smaller-sized models (width = 2.2 nm). However, for larger-sized model (width = 10 nm), the error margin becomes negligible for higher lengths. At higher lengths (above 40 nm), the numerical frequencies are found to be very close (error = ~42%) to analytical values.

zigzag BLGS for bridged case. However, increasing the BLGS length diminishes the effect provided by the atomic configuration. The maximum relative difference calculated as $(\omega_{zigzag} - \omega_{armchair})/\omega_{armchair}$ is of the order of 0.35 and 0.31 for cantilevered and bridged boundary conditions, respectively. In contrast, the difference between the frequencies of the two chiral configurations (i.e., zigzag and armchair) of carbon nanotubes (CNTs) does not show such large discrepancy, with a maximum relative difference for CNTs being of the order of 0.08 [46]. The frequency of CNTs is primarily determined by their geometry [47,48], i.e., diameter and the aspect ratio, and is not significantly altered by varying their atomic structure, especially for long tubes, leading to a general good fidelity of continuum models to predict the vibration of CNTs with different atomic structures. For the case of BLGS, the frequencies seem dependent on both the geometric configuration as well as their chirality for nanostructures with low dimensions.

4.4. Comparison with the continuum theory

The fundamental frequencies obtained from the two equations (reference, Eq. (3)) presented in Section 2 are compared against those from the atomistic-FE models and presented in Fig. 9. The boundary conditions considered in these cases is the simple support at all edges since Eq. (3) takes its simplest form due to the values of coefficients

Table 2
The comparison of numerical results against analytical results. The width considered here is 10 nm. Length unit is in nanometer and the frequency unit is in gigahertz.

Length	$\omega_{AtomisticFE}$	ω[35]
10.9	126.0	153.05
13.4	113.0	130.86
15.9	106.0	118.66
18.3	101.0	111.08
20.8	98.00	105.81
23.2	95.8	102.26
25.7	94.6	99.57
28.2	93.3	97.57
30.6	92.4	96.08

(reference, Table 1) corresponding to this boundary condition. According to the low-dimensional models considered in Fig. 9a, the pattern of variation of natural frequency with length for an atomistic model is found to be dissimilar to that of analytical models. This figure indicates considerable error (~18%) margin for smaller-sized models, as expected when using continuum theories where the equivalent homogenized properties should be averaged over long scales, in particular for the hexagonal lattices of the SLGS. Moreover, finite size SLGS does show orthotropic mechanical properties rather than isotropic as considered in the plate continuum model [17]. For BLGS with larger dimension (Fig. 9b), the atomistic-FE approach provides similar results to the ones predicted by the continuum plate theory. At higher lengths (above 40 nm), the numerical frequencies are found to be very close (error = ~4.2%), giving the evidence of the applicability of the continuum model for relatively large-sized BLGS. From Table 2, we can conclude also that continuum models derived from reference 35 give higher values of the natural frequencies compared to the atomistic-FE model proposed.

5. Conclusions

An atomistic finite element method is proposed for the dynamic analysis of BLGS. In the atomistic-FE model, the C—C bonds are represented by equivalent structural beams with stretching, bending, torsional and deep shear deformation capabilities, based on the equivalence between the harmonic potential expressed in terms of Morse force-field model. The vibrational properties of two types of BLGS (zigzag and armchair) have been investigated using the atomistic finite element approach and continuum plate theory. The mode shapes of SLGS are found to be similar to those of BLGS. It is observed that the BLGS offers a higher bending stiffness compared to SLGSs, leading to higher natural frequencies. Similar to the behavior observed in SLGS, the fundamental natural frequency decreases with increasing length and aspect ratio. The bridged models are found to exhibit higher natural frequencies as compared to cantilever models, making them more suitable for high resonance applications. There is no considerable difference between the dynamic behaviors of armchair and zigzag models for large BLGS configurations, while the chirality affects significantly the dynamic behavior of bilayer graphene for lengths lower than 3 nm.

Acknowledgments

RC and SA acknowledge the support of Royal Society through the award of the Newton International Fellowship and Wolfson Research Merit award, respectively.

References

[1] Y. Gan, W. Chu, L. Qiao, Surf. Sci. 539 (2003) 120.
[2] K.S. Novoselov, A.K. Geim, S.V. Morozov, D. Jiang, Y. Zhang, S.V. Dubonos, I.V. Grigorieva, A.A. Firsov, Science 306 (2004) 666.
[3] M. Ezawa, Phys. Rev. B 73 (2006) (045432:1).
[4] A. Hirsch, Angew. Chem. Int. Ed. 48 (2009) 6594.

[5] H. Santos, L. Chico, L. Brey, Phys. Rev. Lett. 103 (2009) (086801:1).
[6] R. Chowdhury, S. Adhikari, P. Rees, F. Scarpa, S.P. Wilks, Phys. Rev. B 83 (2011) (045401:1).
[7] V.N. Do, P. Dollfus, J. Appl. Phys. 107 (2010) (063705:1).
[8] J.C. Meyer, A.K. Geim, M.I. Katsnelson, K.S. Novoselov, D. Obergfell, S. Roth, C. Girit, A. Zettl, Solid State Commun. 143 (2007) 101.
[9] A. Sakhaee-Pour, M.T. Ahmadian, R. Naghdabadi, Nanotechnology 19 (2008) (085702:1).
[10] R. Chowdhury, S. Adhikari, F. Scarpa, M.I. Friswell, J. Phys. D: Appl. Phys. 44 (20) (2011) 205401.
[11] K.I. Tserpesa, P. Papanikos, Compos. Part B Eng. 36 (2005) 468.
[12] J.B. Oostinga, H.B. Heersche, X. Liu, L.M.K. Vardersypen, Nat. Mater. 7 (2007) 151.
[13] E.V. Castro, N.M.R. Peres, J.M.B. Lopes Dos Santos, F. Guinea, A.H.J. Castro Neto, J. Phys. Conf. Ser. 129 (2008) (012002:1).
[14] H. Hibino, S. Mizuno, H. Kageshima, M. Nagase, H. Yamaguchi, Phys. Rev. B 80 (2009) (085406:1).
[15] A.N. Pal, A. Ghosh, Appl. Phys. Lett. 95 (2009) (082105:1).
[16] A.N. Pal, A. Ghosh, Phys. Rev. Lett. 102 (2009) (126805:1).
[17] F. Scarpa, S. Adhikari, A.S. Phani, Nanotechnology 20 (2009) (065709:1).
[18] S.S. Gupta, R.C. Batra, J. Comput. Theor. Nanosci. 7 (2010) (1546:1).
[19] M.M. Shokrieh, R. Rafiee, Mater. Des. 31 (2010) 790.
[20] F. Scarpa, S. Adhikari, J. Phys. D: Appl. Phys. 41 (2008) (085306:1).
[21] F. Scarpa, S. Adhikari, A.J. Gil, C. Remillat, Nanotechnology 21 (2010) (125702:1).
[22] M. Sadeghi, R. Naghdabadi, Nanotechnology 21 (2010) (105705:1).
[23] F. Scarpa, S. Adhikari, R. Chowdhury, Phys. Lett. A. 374 (2010) 2053.
[24] X.Q. Hea, S. Kitipornchaia, K.M. Liew, J. Mech. Phys. Solids 53 (2005) 303.
[25] R. Chowdhury, C.Y. Wang, S. Adhikari, J. Phys. D: Appl. Phys. 43 (2010) (08540:1).
[26] S. Kitipornchaia, X.Q. Hea, K.M. Liew, Phys. Rev. B 72 (2005) (075443:1).
[27] K.M. Liew, X.Q. He, S. Kitipornchai, Acta Mater. 54 (2006) 4229.
[28] K. Behfar, R. Naghdabadi, Compos. Sci. Technol. 65 (2005) 1159.
[29] I.W. Frank, D.M. Tanenbaum, A.M. van der Zande, P. LMcEuenm, J. Vac. Sci. Technol. B 25 (2007) 2558.
[30] T. Belytschko, S.P. Xiao, R.S. Ruoff, Phys. Rev. B 65 (2002) (235430:1).
[31] E. Cadelano, P.L. Palla, S. Giordano, L. Colombo, Phys. Rev. Lett. 102 (2009) (235502:1).
[32] S. Timoshenko, Theory of Plates and Shells, McGraw-Hill, Inc, London, 1940.
[33] D.J. Gordman, Free Vibration Analysis of Rectangular Plates, Elsevier, New York, 1982.
[34] W. Soedel, Vibrations of Shells and Plates, 3rd ed. Marcel Dekker Inc, New York, 2004.
[35] G.B. Warburton, Proc. Inst. Mech. Eng. Part A J. Power Energy 168 (1954) 371.
[36] R.D. Blevins, Formulas for Natural Frequency and Mode Shape, Krieger Publishing Company, Malabar, FL, USA, 1984.
[37] T. Hull, D.W. Clyne, An Introduction to Composite Materials, Cambridge Solid State Sciences Series, Cambridge Press, 1996.
[38] T. Kaneko, J. Phys. D: Appl. Phys. 8 (1974) (1927:1).
[39] D. Marquardt, SIAM J. Appl. Math. 11 (1963) 431.
[40] J.S. Przemienicki, Theory of Matrix Structural Analysis, McGraw-Hill, New York, 1968.
[41] K.J. Bathe, E.L. Wilson, Numerical Methods in Finite Element Analysis, Prentice-Hall, Englewood Cliffs, NJ, 1976.
[42] L.A. Girifalco, M. Hodak, R.S. Lee, Phys. Rev. B. 62 (2001) 13104.
[43] S. Adhikari, R. Chowdhury, J. Appl. Phys. 107 (2010) (124322:1).
[44] X.L. Feng, R. He, P. Yang, M.L. Roukes, Nano Lett. 7 (2007) 1953.
[45] R.B. Karabalin, X.L. Feng, M.L. Roukes, Nano Lett. 9 (2009) 3116.
[46] R. Chowdhury, S. Adhikari, C.Y. Wang, F. Scarpa, Comput. Mater. Sci. 48 (2010) 730.
[47] R. Chowdhury, S. Adhikari, F. Scarpa, Appl. Phys. A 102 (2011) 301.
[48] R. Chowdhury, C.Y. Wang, S. Adhikari, F. Scarpa, Nanotechnology 20 (2010) (365702:1).